

Computer simulation of coercivity improvement due to microstructural refinement

Hirotoshi Fukunaga,^{1,a)} Ryousuke Hori,¹ Masaki Nakano,¹ Takeshi Yanai,¹ Ryutaro Kato,² and Yoshiyuki Nakazawa²

¹Graduate School of Engineering, Nagasaki University, 1-14 Bunkyo-machi, Nagasaki 852-8521, Japan

²Honda R&D Co., Ltd., 4630 Shimotakanezawa, Tochigi 321-3393, Japan

(Presented 4 November 2014; received 22 September 2014; accepted 9 November 2014; published online 24 March 2015)

The effect of the presence of a non-magnetic phase at multi-junctions of $\text{Nd}_2\text{Fe}_{14}\text{B}$ grains on the demagnetization process of Nd-Fe-B magnets was investigated by micromagnetic simulations, while varying the size of the non-magnetic phase and the $\text{Nd}_2\text{Fe}_{14}\text{B}$ grains. While the demagnetizing field created by the non-magnetic phase assisted the nucleation of a reverse domain, its effect was only significant when its size exceeded a critical value. This critical size effect can be explained by a change in the spatial distribution of the demagnetizing field. In addition, the calculations indicated that microstructural refinement would also increase the coercivity. This increase in coercivity could also be attributed to a change in the spatial distribution of the demagnetizing field due to the presence of a non-magnetic phase. Changes in the spatial distribution of the demagnetizing field due to such a non-magnetic phase could represent a mechanism by which microstructural refinement leads to increased coercivity. © 2015 AIP Publishing LLC.

[<http://dx.doi.org/10.1063/1.4915905>]

I. INTRODUCTION

An increase in the coercivity of Nd-Fe-B magnets is needed to enable their application to electric machines used at high temperatures such as electric and hybrid vehicles, because their coercivity is much lower than their anisotropy field and decreases drastically at high temperatures.¹ Therefore, clarification of the origins of low coercivity is an important issue for the further improvement of coercivity. For example, a reduced²⁻⁴ or negative⁵ magnetic anisotropy constant at grain surfaces, the existence of ferromagnetic grain boundaries,⁶ and a strong local demagnetizing field⁷ have been discussed as candidate origins. It has also been reported that coercivity increases with decreasing grain size.^{8,9} These observations and calculations suggest that the microstructure plays an important role in the determination of coercivity.

Micromagnetic studies have examined the effects of non-magnetic grain boundary phases,¹⁰⁻¹² grain size,¹³⁻¹⁶ and grain surface defects.^{2,3,17} A collective effect of large non-magnetic phases located at the corners of $\text{Nd}_2\text{Fe}_{14}\text{B}$ grains has also been reported for a sintered magnet by computer simulations based on micromagnetic theory.¹⁸ However, these micromagnetic simulations have not clearly determined the effects of the size of the non-magnetic phases.

Therefore, in this investigation, the effect of the presence of a non-magnetic phase at multi-junctions of $\text{Nd}_2\text{Fe}_{14}\text{B}$ grains on the coercivity was studied by varying the sizes of the non-magnetic phase and the $\text{Nd}_2\text{Fe}_{14}\text{B}$ grains. It was

found that the non-magnetic phase decreased the nucleation field remarkably when its size exceeded a critical value. It was also found that microstructural refinement increased the coercivity, which could be attributed to the critical size effect mentioned above.

II. SIMULATION MODEL AND METHOD

A cubic model with a side length L was assumed, as shown in Fig. 1. The model is composed of a $\text{Nd}_2\text{Fe}_{14}\text{B}$ grain, a tetrahedral non-magnetic phase in contact with four $\text{Nd}_2\text{Fe}_{14}\text{B}$ grains, and non-magnetic grain boundaries between two adjacent $\text{Nd}_2\text{Fe}_{14}\text{B}$ grains. The value of L was 48, 96, or 192 nm, and the non-magnetic phase size T was varied over the range from 0 to $0.75 \times L$. The thickness of the grain boundaries was $L/32$. It was also assumed that the thin surface layers of the $\text{Nd}_2\text{Fe}_{14}\text{B}$ grain, which were 3 nm thick, had atomic defects and/or disorder, and the magnetic anisotropy constant for these layers, K_{ud} , was smaller than that for the grain interior, K_u .⁴ An external field was applied along

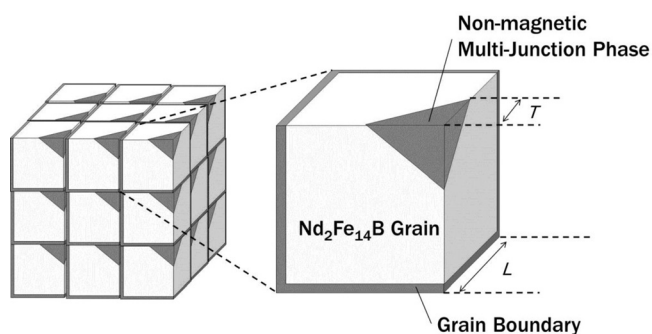


FIG. 1. Calculation model.

^{a)}Author to whom correspondence should be addressed. Electronic mail: fukunaga@nagasaki-u.ac.jp.

TABLE I. Material parameters used in simulation.

	Nd ₂ Fe ₁₄ B	Surface layer	Non-magnetic phase
Anisotropic constant K_u [MJ/m ³]	4.5	2.25 or 4.5	0
Saturation polarization J_s [T]	1.61	1.61	0
Exchange stiffness constant A [J/m]	8.7×10^{-12}	8.7×10^{-12}	0

the easy magnetization direction of the Nd₂Fe₁₄B grain. The model was divided into $32 \times 32 \times 32$ or $64 \times 64 \times 64$ cubic elements, and the element size was either 1.5 or 3.0 nm. Periodic boundary conditions were applied in all three directions, and consequently, an infinitely large magnet was assumed. The assumed physical parameters are shown in Table I.

$$W = K_u^{(H)} V \sum_{i=1}^{N^3} \left\{ \frac{K_{ui}}{K_u^{(H)}} (\mathbf{u}_i \cdot \mathbf{m}_i)^2 - \sum_{j=1}^6 \left[\frac{J_{eij} S}{6K_u^{(H)} V} (\mathbf{m}_i \cdot \mathbf{m}_j) \right] - \frac{M_{si}}{K_u^{(H)}} (\mathbf{m}_i \cdot \mathbf{H}) \right\} + W_m, \quad (1)$$

where K_{ui} and M_{si} are the anisotropy constant and the saturation magnetization of the i th element, respectively. W_m represents the magnetostatic energy due to a local demagnetizing field. N is the total number of elements, whereas S and V are the surface area and volume of each element, respectively. Furthermore, \mathbf{u}_i is a unit vector along the easy axis of the i th element. \mathbf{m}_i and \mathbf{m}_j are the magnetization vectors in the i th and the j th elements, respectively, and are reduced by the saturation magnetization. Moreover, J_{ij} is the exchange interaction constant per unit interface area between the i th and j th elements. The calculation method was described in detail elsewhere.²⁰

III. SIMULATION RESULTS AND DISCUSSION

A. Effect of non-magnetic phase size

At first, the demagnetization process was simulated while varying the size T of the non-magnetic phase from 0 to 72 nm. In this calculation, the model size L was 96 nm, and the magnetic anisotropy constant K_{ud} for the degraded surface layer was $K_u/2$. Figure 2 shows demagnetization curves for $T=6, 30,$ and 72 nm. The volume fractions of the non-magnetic phase for these T value are 0.004, 0.51, and 7%, respectively. The reverse domain was pinned in the degraded surface layer for $T=72$ nm, while magnetization reversal occurred immediately for $T=6$ and 30 nm.

The calculated coercivity h_c and the nucleation field h_n for the above model are shown in Fig. 3 as a function of T . The figure also shows the maximum demagnetizing field h_d present in the Nd₂Fe₁₄B grain in the remanent state. h_c , h_n , and h_d were reduced by the anisotropy field of Nd₂Fe₁₄B ($=2K_u/J_s=5.6$ MA/m). Although h_d increased monotonically with increasing T , the behavior of h_c was classified into

Previously, Rave *et al.* studied the suitable element size for micromagnetic simulation of the switching field at the corner of a grain in which a magnetostatic field plays an important role. They reported that an element size equal to or smaller than the magnetostatic exchange length $\sqrt{2A/(\mu_0 J_s^2)}$ (A : exchange stiffness constant, J_s : saturation polarization, and μ_0 : permeability of vacuum) is sufficient to obtain a correct switching field value.¹⁹ As the magnetostatic exchange length for our model magnet is approximately 2.9 nm, the element size used in our simulation is equal to or smaller than the exchange length. Therefore, our element size should be sufficiently small. In fact, the calculation results using element sizes of 1.5 and 3.0 nm for $L=96$ nm roughly agreed with each other.

The total magnetic energy W stored in the model magnet, when an external field H is applied, is given by

three regions, regions I, II, and III. In region I ($20 \text{ nm} \geq T$), h_c was nearly constant. In region II ($20 \text{ nm} < T < 40 \text{ nm}$), h_c decreased with increasing T and agreed with h_n . In region III ($T \geq 40 \text{ nm}$), h_c was determined by the de-pinning field and was constant. This behavior can be attributed to an effect of the demagnetizing field, because additional calculations neglecting the demagnetizing field resulted in a constant h_c value of approximately 0.61, independent of T .

In region I, increasing T did not affect h_c despite the resulting increase in the demagnetizing field. In order to understand this phenomenon more clearly, one-dimensional calculations were carried out for the model shown in the inset of Fig. 4. The demagnetization field h_d was localized in a region of width W , and a flat external field h_{ex} was applied

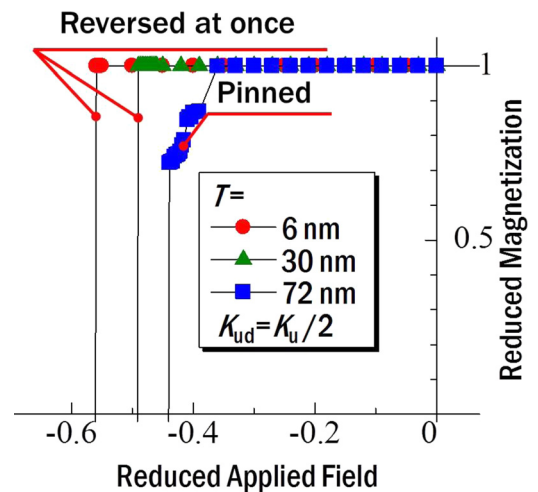


FIG. 2. Demagnetization curves for $L=96$ nm and $T=6, 30,$ and 72 nm. The magnetization and applied field were reduced by the saturation magnetization and the anisotropy field of the Nd₂Fe₁₄B, respectively.

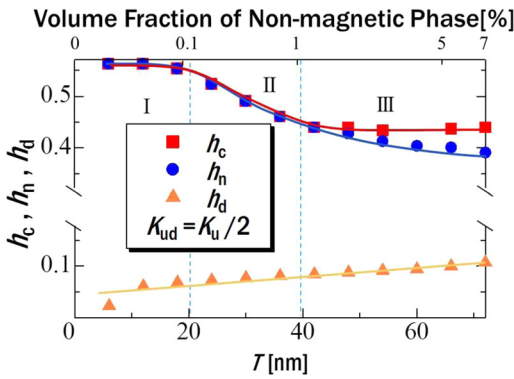


FIG. 3. Coercivity h_c , nucleation field h_n , and the maximum demagnetizing field h_d in the $\text{Nd}_2\text{Fe}_{14}\text{B}$ grain in the remanent state as a function of T . The volume fraction of the non-magnetic phase is also shown in the figure. h_c , h_n , and h_d are reduced by the anisotropy field of the $\text{Nd}_2\text{Fe}_{14}\text{B}$ ($=2K_u/J_s = 5.6 \text{ MA/m}$).

opposite to the direction of magnetization. h_c was calculated by varying h_{ex} under fixed W and h_d values. As seen in Fig. 4, h_c was markedly affected when W reached 10 nm, suggesting that the demagnetizing field had a significant effect on h_c only when it exceeded a critical size. This critical size effect explains the constant h_c value in region I, as shown in Fig. 3.

B. Effect of model size

Figure 5 shows h_c as a function of T/L for $L = 48, 96,$ and 192 nm . The thickness of the degraded surface layer D was kept at 3 nm , and K_{ud} was set to K_u and $K_u/2$ in the calculations shown in (a) and (b), respectively. Clearly, h_c increased with decreasing L . It should be noted that the magnitude of the demagnetizing field for a given T/L value is expected to be nearly the same for all L values, because the geometric configuration of the $\text{Nd}_2\text{Fe}_{14}\text{B}$ grain, non-magnetic phase, and grain boundaries are unaffected by the L value, and the demagnetization field is determined by their configuration rather than their size. For example, the demagnetizing field coefficient does not depend on the magnet size.

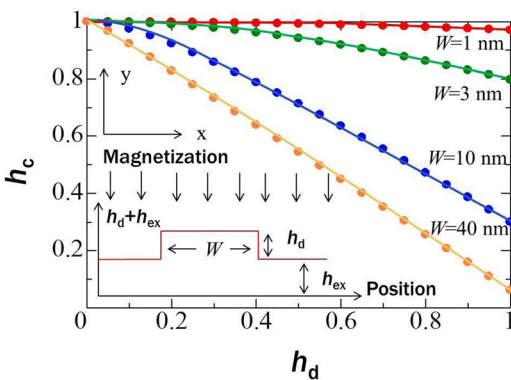


FIG. 4. Coercivity h_c , as obtained by one-dimensional calculations in which the direction of magnetization was assumed to be a function of x . The easy axis of magnetization lies in the $\pm y$ direction, and the magnetization was assumed to initially be in the $-y$ direction. The demagnetization field h_d localized in the region with width W and under a flat external field h_{ex} were applied in the direction opposite to the magnetization (the $+y$ direction). h_c , h_d , and h_{ex} were reduced by the anisotropy field of the $\text{Nd}_2\text{Fe}_{14}\text{B}$ ($=2K_u/J_s = 5.6 \text{ MA/m}$).

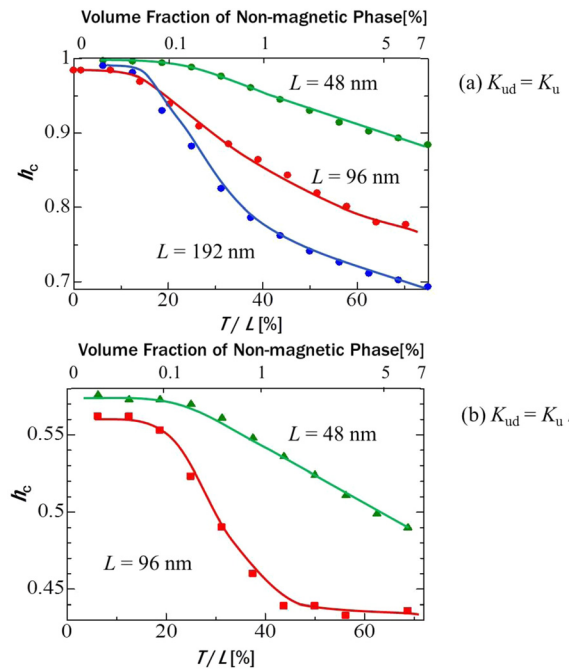


FIG. 5. Coercivity h_c for $L = 48, 96,$ and 192 nm as a function T/L . The magnetic anisotropy constant K_{ud} in the surface layers of the $\text{Nd}_2\text{Fe}_{14}\text{B}$ was set to K_u and $K_u/2$ in (a) and (b), respectively. h_c was reduced by the anisotropy field of the $\text{Nd}_2\text{Fe}_{14}\text{B}$ ($=2K_u/J_s = 5.6 \text{ MA/m}$).

Examples of demagnetizing field distributions in the remanent state are shown in Fig. 6 for $K_{\text{ud}} = K_u$ and $T/L = 0.5$. The demagnetizing field was calculated at a position $L/64$ away from the surfaces of the $\text{Nd}_2\text{Fe}_{14}\text{B}$ grain, as shown schematically in the inset. The distances from the surfaces, $L/64$, correspond to 1.5 nm for $L = 96 \text{ nm}$ and 0.75 nm for $L = 48 \text{ nm}$. The half-width of the h_d vs. position curve for $L = 48 \text{ nm}$ is $1/2$ that for $L = 96 \text{ nm}$, whereas the maximum value of h_d for $L = 48 \text{ nm}$ is the same as that for $L = 96 \text{ nm}$. Therefore, the high h_c values for $L = 48 \text{ nm}$ are consistent because the results shown in Fig. 4 indicate that a narrow distribution of h_d results in a high h_c value for a given h_d value (a given T/L value). It should be noted that the increase in h_c due to the reduction in L can be attributed to a decrease in the size of the non-magnetic phase, which varies

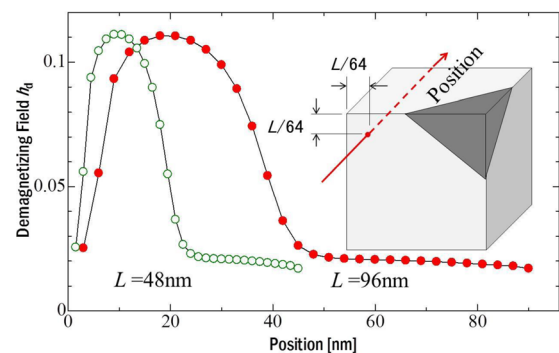


FIG. 6. Examples of demagnetizing field h_d distributions in the remanent state for $K_{\text{ud}} = K_u$ and $T/L = 0.5$. The calculation position is $L/64$ away from the surfaces of the $\text{Nd}_2\text{Fe}_{14}\text{B}$ grain, as shown in the inset. The distances from the surfaces correspond to 1.5 nm for $L = 96 \text{ nm}$ and 0.75 nm for $L = 48 \text{ nm}$. h_d was reduced by the anisotropy field of the $\text{Nd}_2\text{Fe}_{14}\text{B}$ ($=2K_u/J_s = 5.6 \text{ MA/m}$).

proportionally with L . This reduction in the size of the non-magnetic phase may be one origin of the high h_c values that were obtained experimentally for magnets with a small grain size, because refinement of the $\text{Nd}_2\text{Fe}_{14}\text{B}$ grains should accompany the refinement of the non-magnetic phases.

It has already been reported on the basis of micromagnetic simulations that a decrease in grain size increases h_c due to a decrease in the demagnetizing field.¹⁵ This result is not inconsistent with our result because of the difference in the calculation models employed. In the calculations reported in Ref. 15, the grains nearest to the surface of the magnet were assumed to be magnetically soft, and the reversed magnetization in these grains became the source of the demagnetizing field. Consequently, the volume fraction of these grains decreased with decreasing grain size. Therefore, the decrease in demagnetization field can be attributed to the decrease in the volume fraction of magnetically soft grains. In our model, on the other hand, the configuration of the $\text{Nd}_2\text{Fe}_{14}\text{B}$ grain, the non-magnetic phase, and the grain boundaries was the same for $L=48, 96,$ and 192 nm. As a result, the value of h_d was not affected by L . Therefore, our simulation results suggest that a narrow distribution of h_d may be another origin of the experimentally observed increase in h_c due to refinement of the microstructure.

IV. CONCLUSIONS

The effect of the presence of a non-magnetic phase at multi-junctions of $\text{Nd}_2\text{Fe}_{14}\text{B}$ grains on the demagnetization of Nd-Fe-B magnets was studied by micromagnetic simulations. The main findings are summarized as follows:

- (1) The non-magnetic phase created a strong local demagnetizing field and assisted the magnetization reversal. The effect of the demagnetizing field was only significant when the size of the non-magnetic phase exceeded a critical value.
- (2) The critical size effect can be explained by a change in the spatial distribution of the demagnetizing field.
- (3) Microstructural refinement increased the coercivity through a change in the spatial distribution of the demagnetizing field, as mentioned above. The critical size effect represents another origin of the experimentally observed increase in coercivity due to refinement of the microstructure.

¹S. Sugimoto, *J. Jpn. Soc. Powder Metall.* **57**, 395 (2010).

²A. Sakuma, S. Takeda, and M. Endoh, *IEEE Trans. J. Magn. Jpn.* **9**, 127 (1994).

³H. Fukunaga and T. Fukuda, *Jpn. J. Appl. Phys.* **29**, 1711 (1990).

⁴G. Hrkac, T. G. Woodcock, C. Freeman, A. Goncharov, J. Dean, T. Schrefl, and O. Gutfleisch, *Appl. Phys. Lett.* **97**, 232511 (2010).

⁵S. Tanaka, H. Moriya, H. Tsuchiura, A. Sakuma, M. Divis, and P. Novak, *J. Appl. Phys.* **109**, 07A702 (2011).

⁶H. Sepehri-Amin, T. Ohkubo, T. Shima, and K. Hono, *Acta Mater.* **60**, 819 (2012).

⁷H. Kronmüller and K. D. Durst, *J. Magn. Magn. Mater.* **74**, 291 (1988).

⁸Y. Une and M. Sagawa, *J. Jpn. Inst. Metals* **76**, 12 (2012).

⁹P. Yi, M. Lin, R. Chen, D. Lee, and A. Yan, *J. Alloys Compd.* **491**, 605–609 (2010).

¹⁰T. Schrefl, H. F. Schmidts, J. Fidler, and H. Kronmüller, *J. Appl. Phys.* **73**, 6510 (1993).

¹¹D. Süß, T. Schrefl, and J. Fidler, *IEEE Trans. Magn.* **36**, 3282 (2000).

¹²J. Liu, H. Sepehri-Amin, T. Ohkubo, K. Hioki, A. Hattori, T. Schrefl, and K. Hono, *Acta Mater.* **61**, 5387 (2013).

¹³J. Fidler and T. Schrefl, *J. Appl. Phys.* **79**, 5029 (1996).

¹⁴T. Schrefl, H. F. Schmidts, J. Fidler, and H. Kronmüller, *IEEE Trans. Magn.* **29**, 2878 (1993).

¹⁵H. F. Schmidts and H. Kronmüller, *J. Magn. Magn. Mater.* **94**, 220 (1991).

¹⁶H. Sepehri-Amin, T. Ohkubo, M. Gruber, T. Schrefl, and K. Hono, *Scr. Mater.* **89**, 29 (2014).

¹⁷S. Bance, H. Oezelt, A. T. Schrefl, G. Ciuta, N. M. Dempsey, D. Givord, M. Winklhofer, G. Hrkac, G. Zimanyi, O. Gutfleisch, T. G. Woodcock, T. Shoji, M. Yano, A. Kato, and A. Manabe, *Appl. Phys. Lett.* **104**, 182408 (2014).

¹⁸H. Fukunaga, K. Kirino, M. Nakano, and T. Yanai, *J. Jpn. Inst. Metals* **76**, 43 (2012).

¹⁹W. Rave, K. Ramsto, and A. Hubert, *J. Magn. Magn. Mater.* **183**, 329 (1998).

²⁰H. Fukunaga, J. Kuma, and Y. Kanai, *IEEE Trans. Magn.* **35**, 3235 (1999).